HOSTED BY

ELSEVIER

Available online at www.sciencedirect.com

ScienceDirect

Journal of Computational Design and Engineering 3 (2016) 398–413

www.elsevier.com/locate/jcde

Design of a drying system for a rollover carwash machine using CFD

Seyyed M.M. Sabet[a,*], Jorge Marques[b], Rui Torres[b], Mario Nova[b], João M. Nóbrega[c]

[a]*MIT Portugal Program, University of Minho, 4800-058 Guimarães, Portugal*
[b]*Petrotec, Parque Industrial da Ponte, Pav. C2, 4805-661 Guimarães, Portugal*
[c]*Institute for Polymers and Composites (IPC/i3N), University of Minho, 4800-058 Guimarães, Portugal*

Received 29 March 2016; received in revised form 4 July 2016; accepted 5 July 2016
Available online 11 July 2016

Abstract

This work describes the design and development of a new drying system for a rollover carwash machine with the support of numerical tools. The drying system is composed of a pair of stationary vertical dryers and a moveable horizontal dryer that can adjust itself to the contour of a vehicle. After the definition of the dryers' concept, their performance was assessed individually to check their internal flow pattern and to improve their airflow distribution. These issues are expected to provide feedback on redesign and geometric optimization of the dryers. After redesign of the dryers separately, the behaviour of the complete drying system was studied on actual vehicle models, representative of the shortest and tallest dimensions that can be washed with the existing carwash machine sector. The drying efficiency of the whole system was studied by calculation of shear stress distribution on various surfaces of a given vehicle. The results allowed concluding that the overall drying performance of the design system is very good and assure adequate drying on most vehicles surfaces. The results obtained from numerical studies were then validated with experimental measurements and a good agreement was found between the two. The procedure employed in this work can be applied to support the design and analysis of other mechanical drying systems.

Keywords: Rollover carwash machines; Drying system; Computer Aided Design (CAD); Computational Fluid Dynamics (CFD); Shear stress

1. Introduction

Car washes make up a 5 billion dollar a year industry that employs approximately 350,000 people only in the United States and the global market for the car washing services is forecast to reach over $27.4 billion by 2017 [1]. According to a study done by the International Carwash Association, there are more than 3 billion professional washes per year in the US [2]. These statistics highlight the scale and the importance of the car washing industry.

The design of an independent drying system for carwash machines dates back to late 1960s and early 1970s. Cirino's patent [3] encloses one of the earliest designs for a blower equipment of a rollover carwash in 1976. Schleeter et al. [4] patented a concept based on a drying system and stripper cloth. Larson et al. [5] proposed a drying equipment for an automatic carwash composed of two vertical dryers and a top horizontal one, similar to the most current carwash dryers. Belanger et al. [6] gave one of the earliest drying systems concepts in which the dryer can adjust itself to the contour of the vehicle. Other patent works [7,8] developed automatic control systems and electronic devices for car washing dryers.

One of the main design patents for a rollover carwash was proposed by Schleeter [9], which is a portable apparatus comprising of an upright U-shaped system. In this invention, the vehicle is held stationary at a designated position between rails and a travelling frame moves on the rails past the vehicle body. The travelling frame is first moved in one direction so that the body is washed, and then in reverse to dry the vehicle. Fig. 1 shows an automatic rollover carwash machine that works based on the same approach manufactured by the company in which this work was carried out.

*Corresponding author.
E-mail addresses: smm.sabet@gmail.com, sabet@dem.uminho.pt (S.M.M. Sabet).
Peer review under responsibility of Society of CAD/CAM Engineers.

http://dx.doi.org/10.1016/j.jcde.2016.07.001

Fig. 1. The front and rear views of a recent rollover carwash machine.

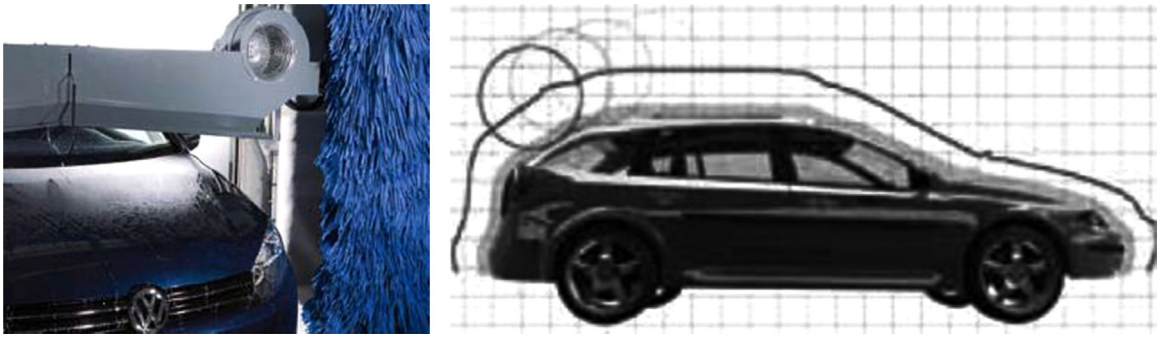

Fig. 2. The horizontal dryer position relative to a vehicle's contour [10].

The architecture of the drying system of the present rollover car washing machines is composed of two fixed vertical dryers on the sides, which are accommodated in the columns and fed by two centrifugal fans, and also a movable horizontal dryer with two centrifugal fans mounted at each end. While the vertical dryers are fixed and mounted to the structure, the horizontal dryer can move vertically and is controlled by a set of sensors, which detect the presence of a vehicle on the washing bay and enable the dryer to follow its contour and precisely position relative to its surface [6], as shown in Fig. 2 from a major carwash manufacturer, the distance from the tip of the horizontal dryer to the vehicle's surface is adjustable and usually set between 10 and 20 cm [8].

Understanding the mechanism of water droplet expulsion from surfaces provides a useful guidance for an efficient design of the drying system and evaluating its efficiency. The adhesion of a droplet onto a solid surface is observed in two types: (1) normal and (2) lateral. The normal adhesion is the adhesion required to detach a droplet from a substrate in perpendicular direction, such as the force to cause the droplet to fly off from the surface. The lateral adhesion refers to the force required to slide a droplet on the surface, for example, to move it to another location [11]. The most relevant mechanism for water droplet expulsion, for drying of a vehicle, is the lateral adhesion. The relation between a droplet diameter and airflow velocity required to detach it, has been the subject of several studies [12–15]. The available relations [12,13] were adapted in this work to obtain a relation between the wall shear stress and the droplet expulsion, and were used to evaluate the drying efficiency of the new drying system designed in this work.

The ideal drying system of a carwash machine effectively forces the water droplets downwards away from the roof and sides of the vehicle. However, as the geometry of the vehicle, its surface topography and the distance between the car and the rollover vary from one vehicle to another, there is no perfect design for a dryer that can be efficient for all vehicle types. Consequently, there is usually a trade-off between the quality of the drying and the vehicle size/type. One of the main drawbacks of the most rollover dryers is inadequate drying performance on the lower lateral regions of the vehicle close to the bumpers and rocker panels.

There is no report on the performance assessment of car washing drying system using numerical methods in the literature. The objective of this work is to design a new drying system for a rollover carwash machine in order to improve lateral drying efficiency, while maintaining a satisfactory drying on the horizontal and roof surfaces using numerical

tools. Also, the drying efficiency of the new design concept is to be improved by redesign and optimization.

Initially the new drying system concept is presented. The boundary conditions, the computational domain, and meshing used in the numerical studies are later explained. Then a water droplet expulsion criterion is established as an index for evaluating the drying efficiency of the new concept. Then, the results are presented for individual dryers and the full drying system. Finally the conclusions drawn from numerical studies are presented and compared with experimental measurements.

2. Drying system design

Both horizontal and vertical dryers are intended to have an efficient airflow to expel all water droplets on different vehicle surfaces, and therefore they need to be designed in a way to identify their optimum geometry. The main objective of the design of a drying system is to maintain a better airflow velocity and distribution pattern over vehicle surfaces.

The geometry of the dryers is restricted to the overall dimensions of the rollover machine; how the drying system is connected and supported by the structure; and the internal space inside the structure that accommodate the dryers. Fig. 3(a, b) shows the vertical and horizontal dryers concept developed for this work. Both dryers are equipped with 3 kW fans (the technical features of the fans used in the dryers are presented in Annex 1). The horizontal dryer's outlet has an area of 1850×18 mm^2, while that of the vertical ones is 1100×18 mm^2.

Fig. 3(c) shows a schematic layout of the entire drying system relative to a given vehicle. The four circles, whose centers are marked with stars (*), represent the ventilator fans.

As the efficiency of new drying system is to be determined, a set of numerical studies was carried out to evaluate the effectiveness of the drying on various vehicles. In order to simplify the model and to save computational time and resources, the ventilator's fans were deleted and instead their equivalent flow rates were considered at their outlets. The inlets have the exact same inlet flow properties of the engines; and therefore this simplification is not expected to have any effect on the accuracy of the results. Fig. 3(d) shows the standard views of the drying system simplified for numerical studies.

3. Case studies

In order to study the drying effectiveness of the new drying system for droplet removal, a number of numerical studies were carried out. Initially, the horizontal and vertical dryers were modelled individually to study their internal flow pattern, and then the efficiency of the complete drying system for water

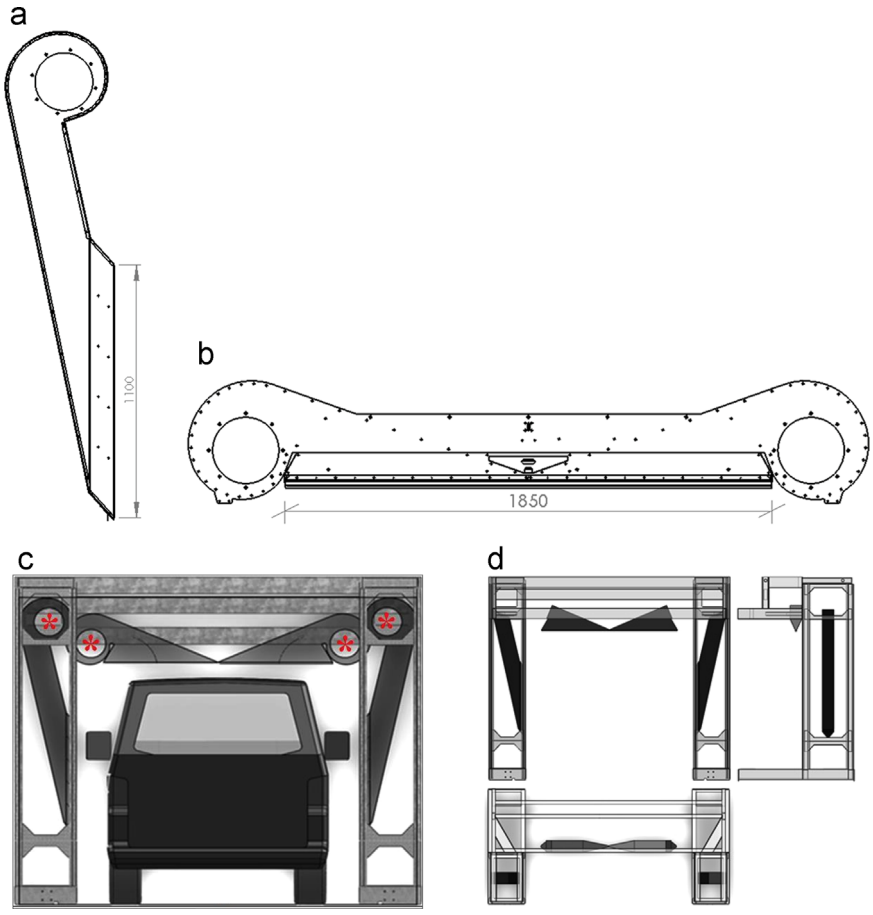

Fig. 3. (a) The vertical dryer concept, (b) the horizontal dryer [dimensions in mm], (c) the position of the entire drying system relative to a vehicle, (d) the standard views of the drying systems implified for numerical studies.

droplet removal from actual vehicle surfaces was studied and analysed by calculation of shear stress distribution on various vehicle surfaces. The results obtained from numerical studies were then compared against experimental measurements.

3.1. Fluid flow model

The numerical studies were performed in SOLIDWORKS Flow Simulation. The air was selected as the fluid in the general setting of the software. The fluid flow inside the internal duct system is incompressible. All the calculations were done at room temperature (20 °C) and the heat conduction was disabled in the software (mechanical drying).

The flow model used in this work is in steady state, as the magnitude and direction of dryer's airflow is constant throughout the computational domain with respect to time (versus the transient flow where the magnitude or direction of the flow changes over time).

The *External* analysis was used, which concerns the flow not bounded by outer solid surfaces, but only by the computational domain boundaries. If one wants to analyse both internal and external flows simultaneously, the analysis is treated as an *External* one. In this case, the solid model (or the carwash machine) is surrounded by the flow.

SOLIDWORKS solver is based on the Navier–Stokes equations, as formulations of mass (Eq. (1)), momentum (Eq. (2)) and energy (Eq. (3)) conservation laws [16]:

$$\frac{\partial \rho}{\partial t} + \frac{\partial(\rho v_i)}{\partial x_i} = 0 \tag{1}$$

$$\frac{\partial(\rho v_i)}{\partial t} + \frac{\partial}{\partial x_j}\left(\rho v_i v_j\right) = \frac{\partial \tau_{ij}}{\partial x_j} - \frac{\partial p}{\partial x_i} \tag{2}$$

$$\frac{\partial(\rho E)}{\partial t} + \frac{\partial}{\partial x_j}\left(\rho v_j E\right) = \frac{\partial}{\partial x_j}\left(k\frac{\partial T}{\partial x_j}\right) + \frac{\partial}{\partial x_j}(\tau_{ij} v_i) \tag{3}$$

SOLIDOWORKS is able to consider both laminar and turbulent flows. Laminar flows occur at low Reynolds numbers, while turbulent ones have higher Reynolds values. The turbulent flows are solved by the Favre-averaged Navier-Stokes equations. Based on the literature [17], the ventilators flow (used in this work) is a medium turbulence case in which turbulence intensity is in the range of 1–4%, which was considered in all the case studies of this work.

3.2. Drying system computational model

As the behaviour of the employed fans is known (flow rate: 2830 $m^3\ h^{-1}$), they were not considered in the computational model. An imposed flow rate boundary condition was considered in the numerical model, by using the fan flow rate obtained from their datasheet (Annex 1).

In order to define the boundary conditions, a flat surface large enough to cover the whole computational domain was created which acts as the floor (shown in Fig. 4). The no-slip boundary condition [18] was applied on the computational domain surfaces. Due to symmetry reasons and in order to save computational time and resources, only half of the domain was considered in all the studies. The computational domain and boundary conditions employed for the horizontal and vertical dryers are presented in Fig. 4(a) and (b), respectively. The full drying system was also simulated in a similar manner using symmetry conditions.

3.3. Computational mesh

SOLIDWORKS flow simulation has the ability to adapt the computational mesh to the solution during the calculation. The solver splits the mesh cells in regions with high-gradient flow and merges the cells in the low-gradient ones, yielding more accurate results, while minimizing the computational effort [19].

For the mesh sensitivity analysis of the horizontal dryer, 4 different mesh levels (coarse: M1, medium: M2, fine: M3

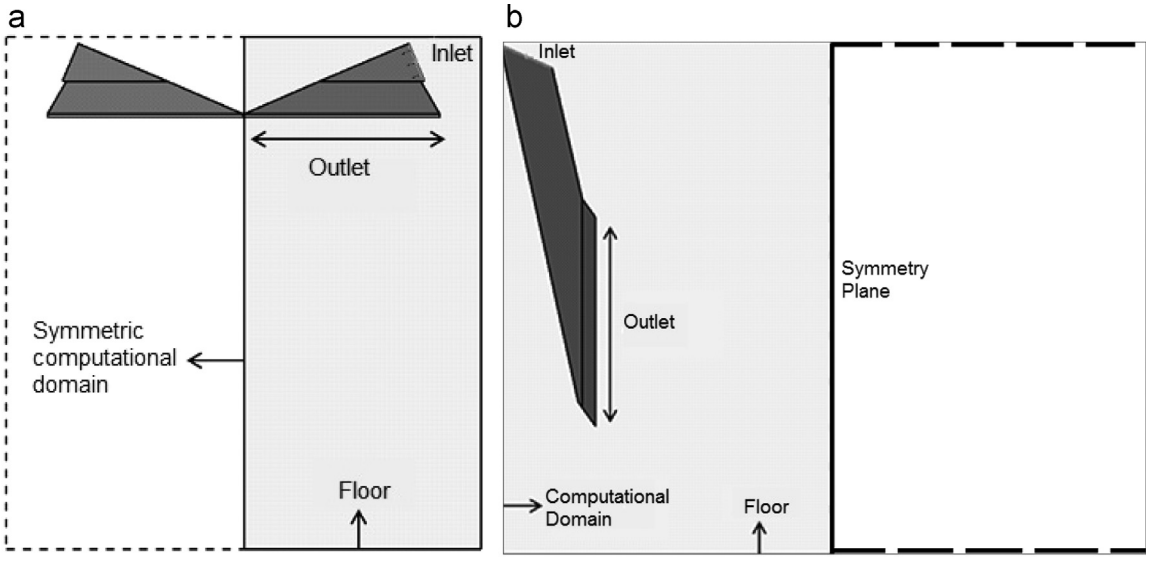

Fig. 4. The boundary conditions and computational domain used for (a) horizontal and (b) vertical dryers.

Table 1
The number of cells (in thousands) for the mesh sensitivity analysis of the horizontal dryer.

Mesh level		M1	M2	M3	M4
Number of cells	Fluid	10.6	83.4	486.3	940.9
	Solid	0	0	0.2	33.5
	Partial	4.9	37.1	190.4	414.9
	Total	15.5	120.6	677	1389

Table 2
The number of cells (in thousands) for the mesh sensitivity analysis of the vertical dryer.

Mesh level		M1	M2	M3	M4
Number of cells	Fluid	7.8	51.1	473	1027
	Solid	0	0	6.5	76.9
	Partial	3.5	29.323	195.3	408.1
	Total	11.3	80.5	675	1512

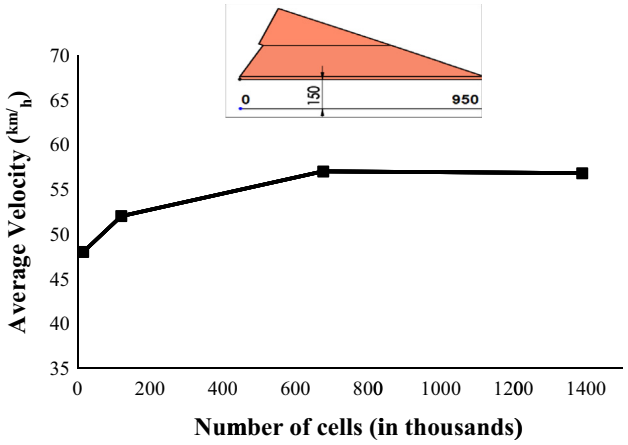

Fig. 5. The average airflow velocity of the horizontal dryer versus the number of cells (distance: 150 mm).

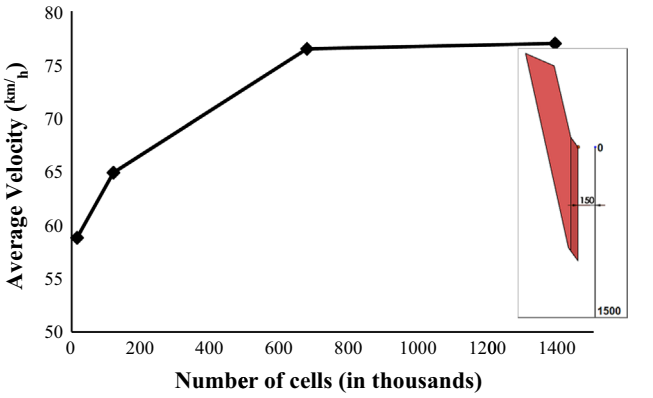

Fig. 6. The average airflow velocity of vertical dryer versus the number of cells (distance: 150 mm).

and very fine: M4) were used. M2 meshing had about 2 times the number of cells in each direction (8 times in volume) than M1, while M3 had 4 times the number of cells in each direction than the coarse one and 64 times in volume. For M4, the number of cells was nearly twice that of M3. The number of cells after meshing fluid, solid and partial regions is listed in Table 1. The partial cells in Table 1 (and the rest of the paper) refer to those that have some of their volume occupied by a solid and the rest with the fluid, while the other two are occupied with only solid or fluid.

The mesh sensitivity analyses were based on calculation of average velocity versus mesh quality. Fig. 5 shows the average velocity on the mid-plane of the horizontal dryer at a 150 mm distance from its outlet (shown with an index above the figure). As it can be seen, the average velocity is nearly the same for M3 and M4. Based on the results, it was concluded that M3 and M4 are accurate for the studies on the horizontal dryer. The final mesh selected (M3) contained approximately 486,000 fluid, 190,000 partial and 677,000 total cells.

The same meshing strategy was applied for the vertical dryers. Similarly, 4 different mesh levels (M1, M2, M3, M4) were used. The mesh M2 had twice the number of cells of M1 in each direction (8 times in volume). The total number of cells in M3 and M4 was approximately 64 and 128 times than the number of cells in M1. Table 2 lists the number of cells in each meshing level.

Fig. 6 shows the average airflow velocity on the mid-plane of the vertical dryer at a 150 mm distance along the outlet (shown with an index). As it can be seen, the average velocity

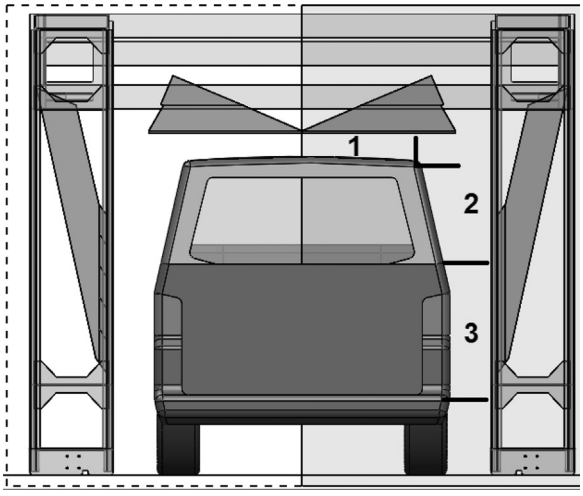

Fig. 7. The surfaces studied for the mesh sensitivity analysis of the full drying system.

is nearly the same for M3 and M4. Based on the results, mesh M3 was selected for all the studies on the vertical dryers. This mesh contained approximately 473,000 fluid, 195,300 partial and 675,000 total cells.

The mesh sensitivity analysis for the complete drying system was based on plotting the average shear stress on the external vehicle surfaces that are important in the drying stage. These surfaces are shown and named in Fig. 7 on a simplified Volkswagen pickup van as 1, 2, 3 (roof-top, side window and door/rocker panels, respectively).

For the sensitivity analysis studies of the full drying system, six different meshing levels were used, as listed in Table 3.

Fig. 8 shows the average shear stress for the three surfaces shown in Fig. 7 as the number of cells (or mesh quality). As it can be seen, the plot remains constant for the three surfaces after approximately 1.5 million cells. As the result, the final mesh selected for the full drying system was M5 that contained approximately 1,160,000 fluid, 409,000 partial and 1,610,000 total cells.

Fig. 9 shows the final meshing selected for the horizontal, vertical and the full dryers. As it can be seen, the mesh surrounding the dryer is fairly coarse, but in regions of solid/fluid interfaces is much finer to improve the accuracy of the results where it is needed. This mesh has nearly 10 cells across the outlet channel in all the cases.

Table 3
The number of cells (in thousands) for the mesh sensitivity analysis of the full drying system.

Mesh level		M1	M2	M3	M4	M5	M6
Number of cells	Fluid	17.9	30.2	167.5	376.7	1163	1879
	Solid	3.9	8.3	11.5	9.9	37.3	98.6
	Partial	11.5	23.7	89.4	179.0	409.9	650.7
	Total	33.4	62.2	268.5	565.7	1610	2628.3

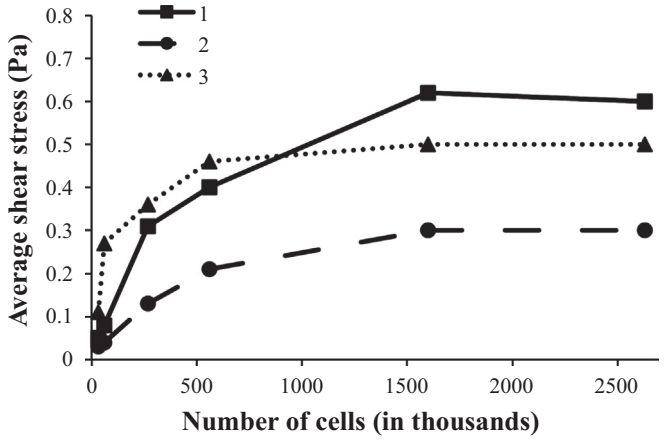

Fig. 8. The average shear stress distribution versus number of cells on the three surfaces (1, 2, 3) shown in Fig. 7.

3.4. Selection of the computational domain

The effect of computational domain size on the accuracy of the numerical results was studied for the individual and the full drying system. For this means, the horizontal and vertical dryers with 3 different computational domain sizes: small (CD1), medium (CD2) and large (CD3) were investigated. For the full drying system, two different computational domain sizes were studied: small (CD1) containing only the dryers and the desired region around the dryers and large (CD2) which contained the entire vehicle length. The same meshing, selected after the sensitivity analyses were used in all the studies. The results showed that the computational domain size does not affect the accuracy of the results [2].

3.5. Water droplet expulsion criterion

For a given fluid moving along a solid boundary, due to the flow restriction promoted by the boundary, there is a shear stress caused by the fluid on that boundary layer [18]. The shear stress over a given face is representative of water droplet expulsion on that face [20]. In order to convert the equivalent

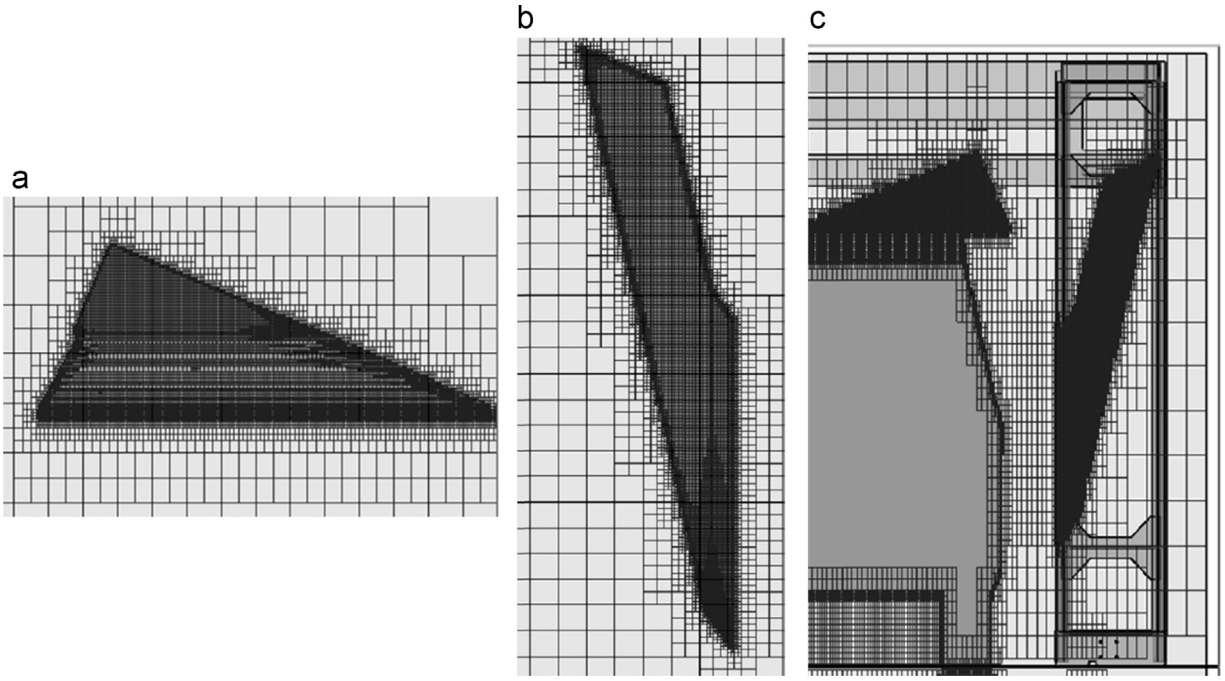

Fig. 9. The final mesh selected for (a) the horizontal, (b) vertical and (c) the full dryer studies.

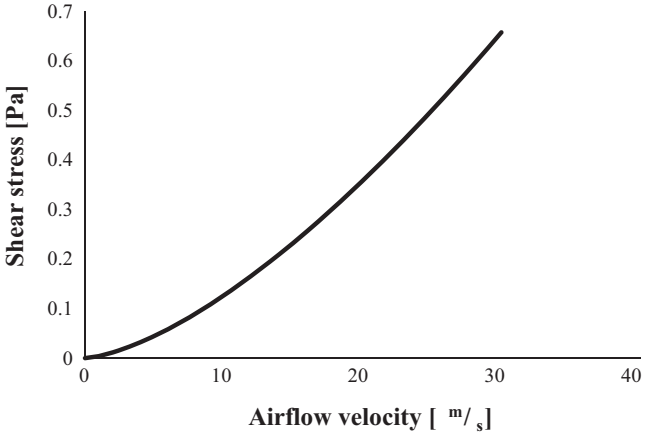

Fig. 10. The shear stress versus airflow velocity (distance: 150 mm).

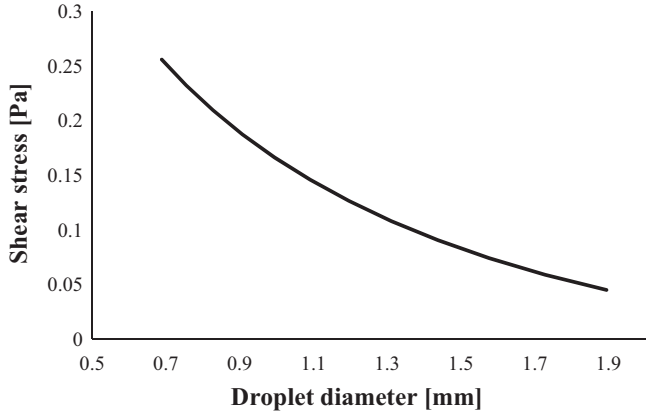

Fig. 11. The shear stress required for expulsion of water droplets on horizontal solid surfaces.

airflow velocity over a surface into the shear stress caused on a surface, Blasius equation [21] is used:

$$\tau_{xy} = \frac{0.332\rho V^2\sqrt{\upsilon}}{\sqrt{V.x}} \tag{4}$$

where υ is the kinematic viscosity of the air (1.51×10^{-5} m^2/s at 20 °C), ρ the density of air (1.2 kg/m^3 at 20 °C), x distance and V denotes the airflow velocity [22]. Eq. (4) can be re-written to express airflow shear stress at 20 °C, as follows:

$$\tau_{xy} = \frac{0.001547V^2}{\sqrt{V.x}} \tag{5}$$

Eq. (5) gives the shear stress as a function of airflow velocity and distance. Fig. 10 shows the relation between shear stress and airflow velocity obtained from Eq. (5) at the distance of 150 mm (the relative distance of the dryers to the vehicle).

Theodorakakos et al. [13] results for airflow velocity versus droplet diameter were used in order to obtain the relation between shear stress and the droplet size. By substituting the shear stress at a given airflow velocity (from Fig. 10), the relationship between the shear stress as a function of droplet diameter may be obtained.

Fig. 11 shows the resulting plot of shear stress versus water droplet diameter obtained at a distance of 150 mm. As the droplet becomes larger, the drag force increases rapidly as compared to the holding surface tension force, which explains the negative slope of the plot in Fig. 11.

Fig. 11 can be used as index for water droplet expulsion from surfaces of the vehicles. The area above this curve is the safe region for water droplet expulsion; meaning that for a given droplet size, the shear stress values higher than this curve would remove that droplet. For instance, a shear stress of approximately 0.17 Pa is required to detach a 1 mm droplet on a horizontal surface. For the case of vertical surfaces, as gravity is in favour of the detachment, the required shear stress value for droplet removal is even lower that the curve presented here. As the result, the drying is effective in both horizontal and vertical surfaces, as long as the shear stress value is above the curve shown in Fig. 11.

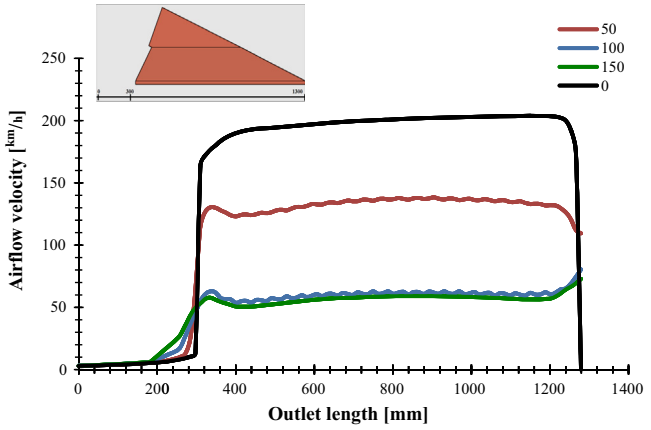

Fig. 12. The velocity profile along the horizontal dryer outlet at different distances from the outlet.

3.6. Studies performed

Initially, the horizontal and vertical dryers were studied separately. The main purpose of these studies was to check the effect of the shape and geometry on the overall performance of each dryer. Also, the complete drying system was studied to ensure the efficiency of the drying system and expulsion of water droplets from the vehicle surfaces. Two representative car geometries of Volkswagen pickup van and Smart were considered. The drying efficiency was studied on these two vehicles because they are representatives of the shortest and tallest vehicles (1500 and 2100 mm, respectively) that can be used in the carwash machine (the overall dimensions of these two vehicles is presented in Annex 2).

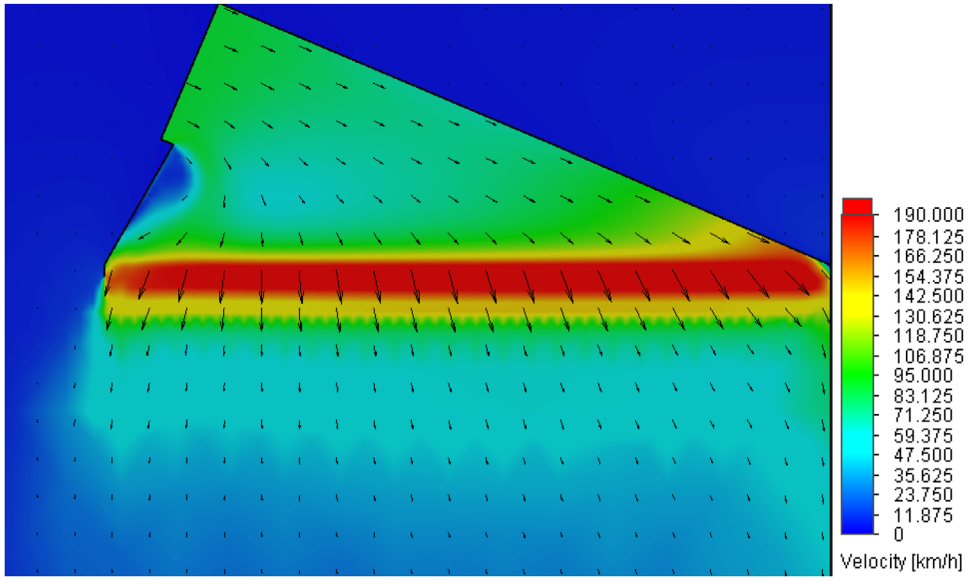

Fig. 13. The velocity distribution on the mid-plane of the horizontal dryer.

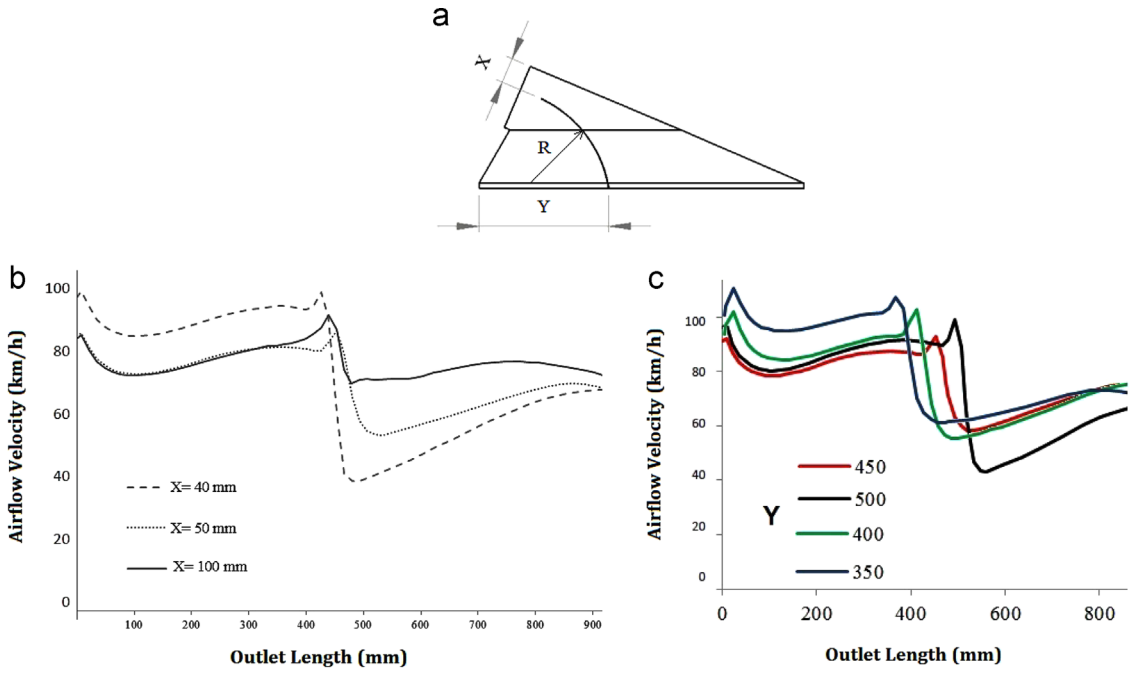

Fig. 14. The position of the internal flap inside the horizontal dryer (a). The velocity profiles obtained from horizontal dryer for various *X* (b); and *Y* (c) values (distance: 150 mm).

4. Results and discussion

4.1. Horizontal dryer

Fig. 12 shows the airflow velocity profiles obtained at 0, 50, 100, 150 mm distances from the horizontal dryer outlet.

Fig. 13 shows the velocity distribution on the mid-plane of the horizontal dryer. The arrows represent the velocity direction and their size is the magnitude of velocity. It can be seen that the velocity drops down near the left side of the dryer.

In order to improve the drying on the lateral sides of the vehicle, an attempt was made to direct the airflow inside the horizontal dryer using an internal flap. As shown in Fig. 14(a), the distance of the flap to the upper edge and the farthest outlet corner (*X* and *Y*) were defined by a trial and error method through a set studies and analysis of the resulting airflow pattern and velocity profile of the dryer.

A number of these studies are presented in Fig. 14(b, c), which show the velocity profiles (at a distance of 150 mm) for various *X* and *Y* values. The studies showed that reducing *X*,

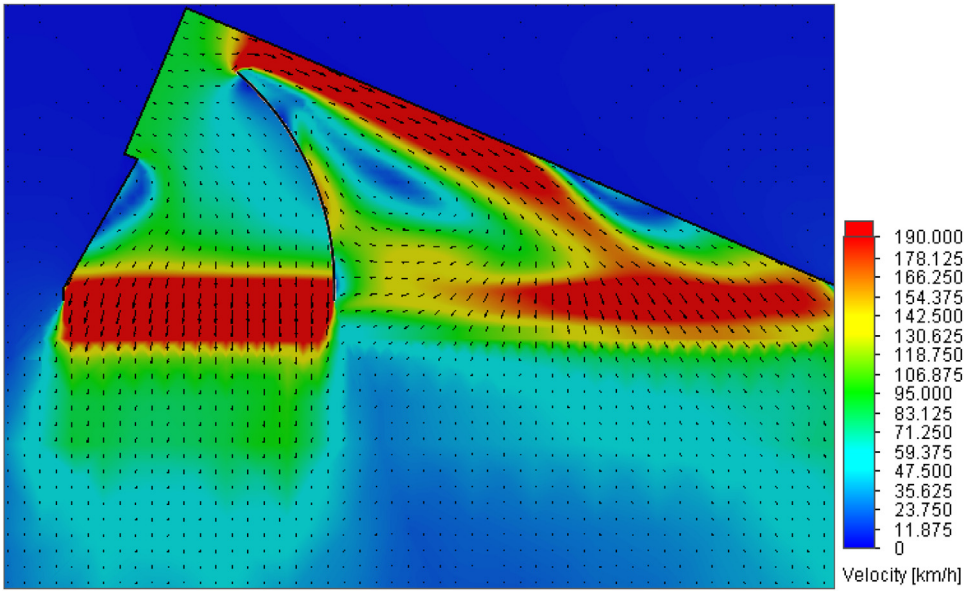

Fig. 15. The velocity distribution on the mid-plane of the proposed horizontal dryer with flap.

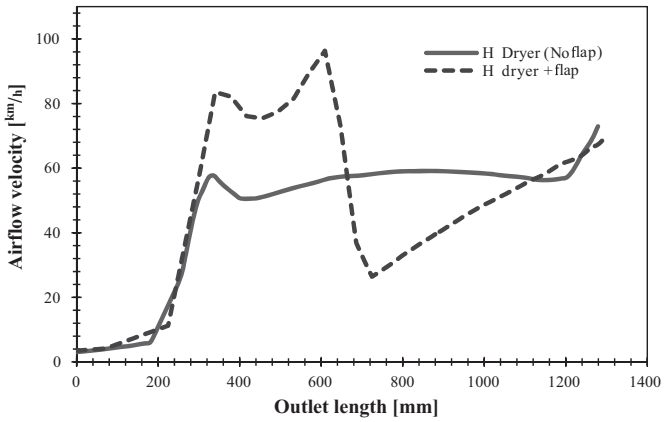

Fig. 16. The airflow velocity profile of the horizontal dryer without/with flap along its outlet (distance: 150 mm).

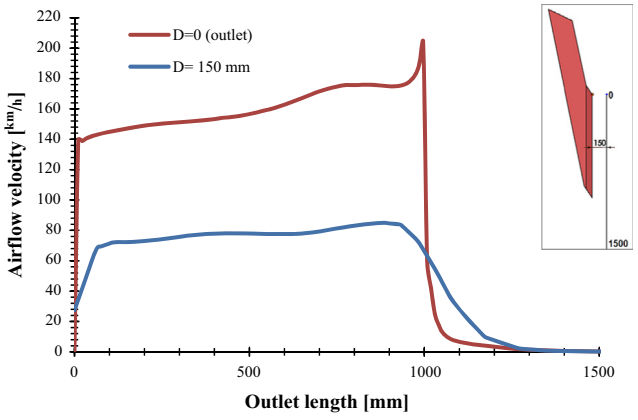

Fig. 17. The airflow velocity profile of the vertical dryer along its outlet at 0 and 150 mm distances.

reinforces the airflow in the corner, while reduces that in the middle. Additionally, increasing X, reduces the effect of the flap. Also, Y cannot be too large, since it will not have any effect for reinforcing the airflow in the corner and cannot be too short either, as it will block the approaching airflow and cause recirculation.

The flap with $X=60$ mm, $Y=350$ and $R=350$ mm was shown to improve the airflow velocity in the left corner, while maintaining a satisfactory one in the right side. Fig. 15 shows the velocity distribution on the mid-plane of the horizontal dryer with the optimized flap. As it can be seen the velocity is reinforced in the region between the flap and the left corner where it is expected to help lateral drying.

Fig. 16 shows the airflow velocity profiles at 150 mm distance from horizontal dryers with and without flap. As it can be seen, the velocity is reinforced about 25–30 km/h in the region between the flap and the corner; however, it has decreased after the flap.

4.2. Vertical dryer

The vertical dryers play an important role in drying lateral surfaces of the vehicle. If the airflow is directed towards the side mirrors, instead of lower regions such as wheels and bumpers, these regions will be left with water droplets on them. If their airflow is pushed downwards, the side glass and mirrors will not be dried effectively. As the vertical dryers are fixed inside the structure of the rollover machine, their distance to the vehicle depends on the width of the vehicle. This

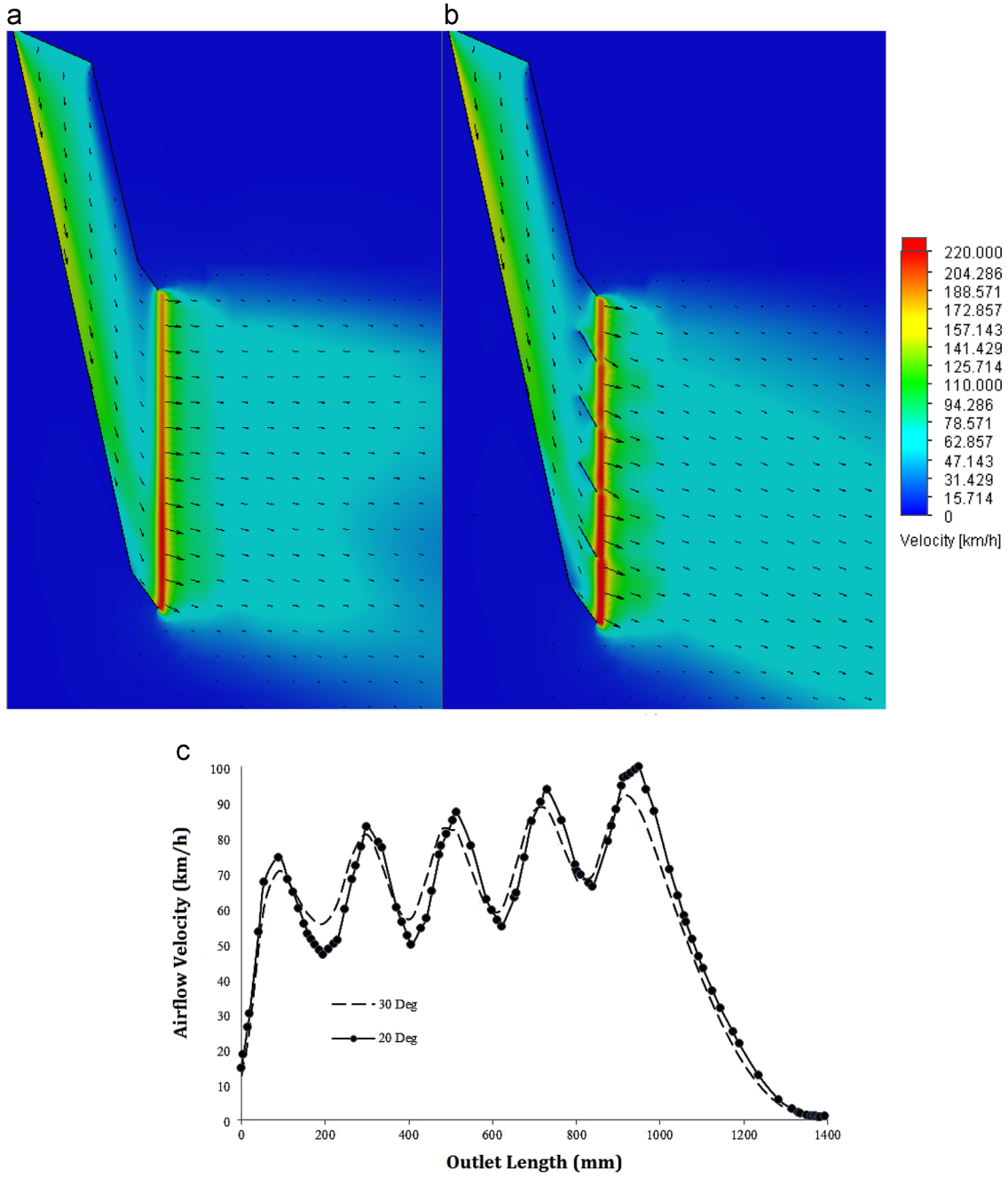

Fig. 18. The velocity distribution on the mid-plane of the vertical dryer (a) without and (b) with the proposed flaps. (c) The airflow velocity profiles of the vertical dryer along the outlet with 201 and 301 flaps (distance:150 mm).

distance was considered about 150 mm based on the largest vehicle in the car flit segment.

Fig. 17 shows the velocity profile of the vertical dryer obtained at the outlet (0 mm) and 150 mm distance from the outlet. It can be seen that the velocity at the outlet ($D=0$ mm) is slightly increasing from the upper tip of the outlet to the lower one. This is while the velocity is nearly constant at 150 mm in this region.

Fig. 18(a) shows the velocity plot on the mid-plane of the vertical dryers. As it can be seen, the velocity is higher at the left side of the duct as compared to the right side.

An attempt was made to improve the airflow pattern of the vertical dryer using internal flaps to direct the airflow as desired. Similar to the horizontal dryer case study, several trial and error experiments were carried out to define the optimum geometry and number of flaps. An example of these studies is presented in Fig. 18(c), which compares the airflow velocity of the vertical dryers along their outlets at 150 mm distance with 20° and 30° flaps.

The results showed that the most effective flaps are the ones at the outlet duct. A set of 4 flaps was aligned in a way to make a 45° angle with the dryer's outlet and have the same

distance from each other (200 mm). Running the same study with the vertical dryer with the optimum flaps showed a better distribution as illustrated in Fig. 18(b). It can be seen that the internal flow is very similar in the two cases, but the external airflow distribution has been pushed downwards and directed towards lower areas of the vehicle. This is important for drying the rocker panels and lower regions (close to the ground) where lack of drying efficiency is usually observed in most car washing machines.

Fig. 19 shows the airflow velocity profiles at 150 mm distance from vertical dryers with and without proposed flaps. It is notable that due to the law of mass conservation, it is not possible to increase the airflow velocity in all the regions for the proposed dryer with flaps. Therefore, as it can be seen in Fig. 19, the velocity is higher at the tip of the flaps (peaks) and lower in the regions in-between.

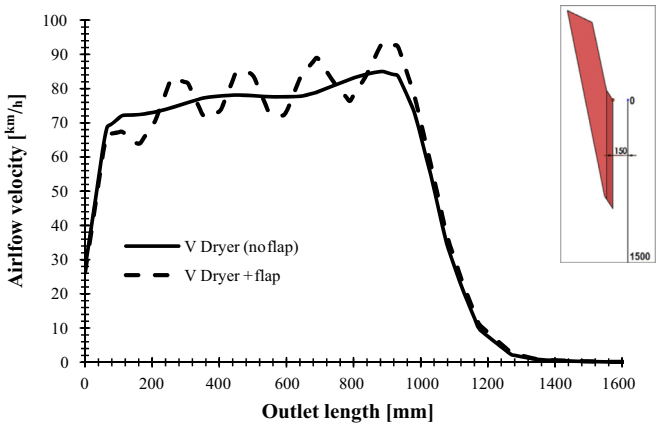

Fig. 19. The airflow velocity profiles along the outlet of the vertical dryer without/ with flaps (distance: 150 mm).

4.3. Full drying system

4.3.1. Drying performance on Volkswagen van

Fig. 20 shows the shear stress distribution with the proposed drying system on the lateral and roof surfaces of the Volkswagen pickup van (VW). It can be seen that shear stress at the immediate impacted regions of the outlets is lower as compared to the areas surrounding it. Since the vehicle is stationary and the rollover is moving along, the regions with lower shear stress will be covered by higher values by the passage of the drying system.

The same figure evidences that drying on the roof and lateral glass and doors is very effective. This refers to the area marked in Fig. 20(b). The shear stress level on the rocker panels is lower than upper parts and is in the range of 0.95–3 Pa, which is in the safe area of Fig. 11 for water droplet expulsion on horizontal surfaces.

Fig. 21 shows shear stress distribution of the frontal parts (bumper and headlight surfaces) on the same VW. As it can be seen, the shear stress is very well distributed on the lateral sides in both cases and therefore drying is expected to be very effective in these regions. Fig. 21(b, c) shows the shear stress on the headlights. It can be seen that shear stress here is enough for water expulsion; however, the lower edges of bumpers and rocker panels possess lower shear stress values, as compared to headlights. This limitation is not a design

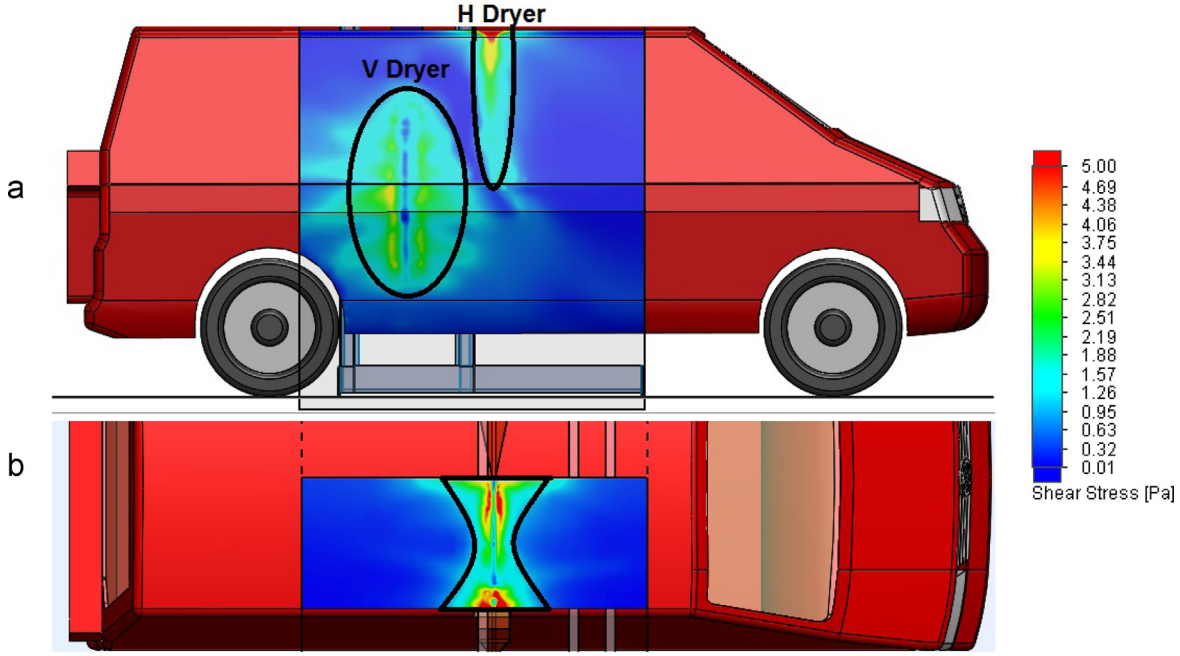

Fig. 20. The shear stress distribution on (a) the lateral and (b) rooftop surfaces of Volkswagen.

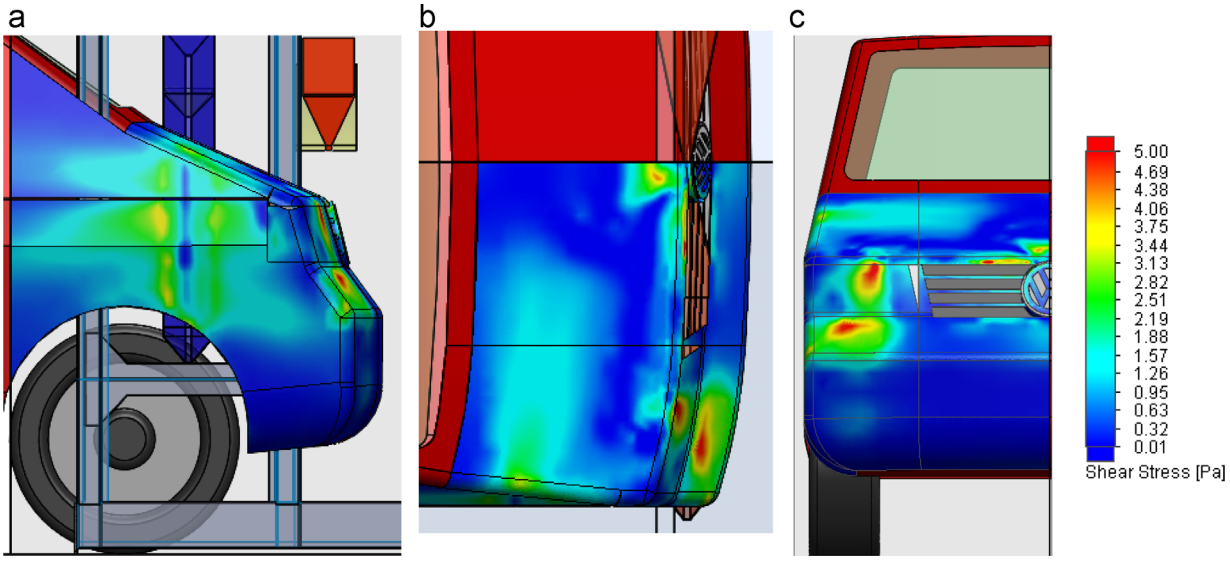

Fig. 21. The shear stress distribution on the lateral (a) and frontal (b, c) surfaces of Volkswagen.

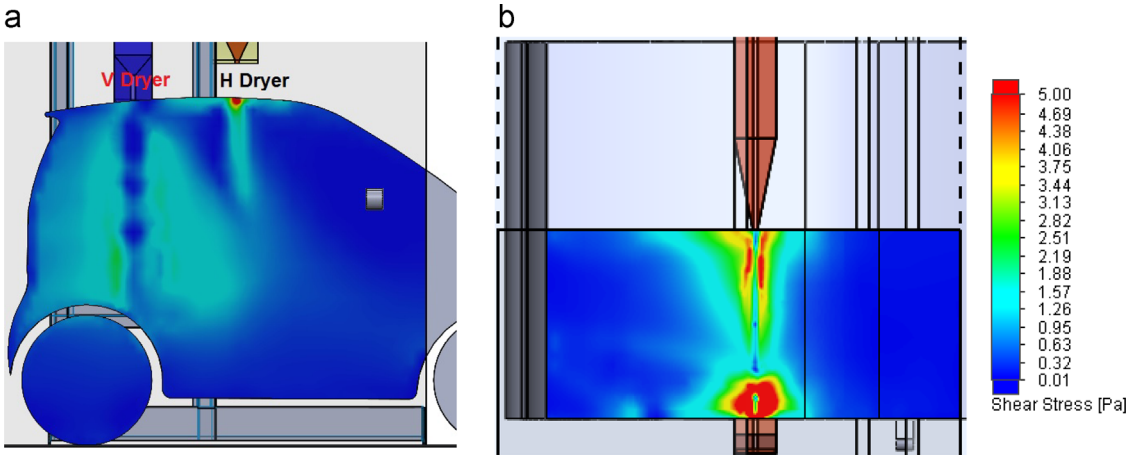

Fig. 22. The shear stress distribution on the lateral (a) and roof top (b) surfaces of Smart.

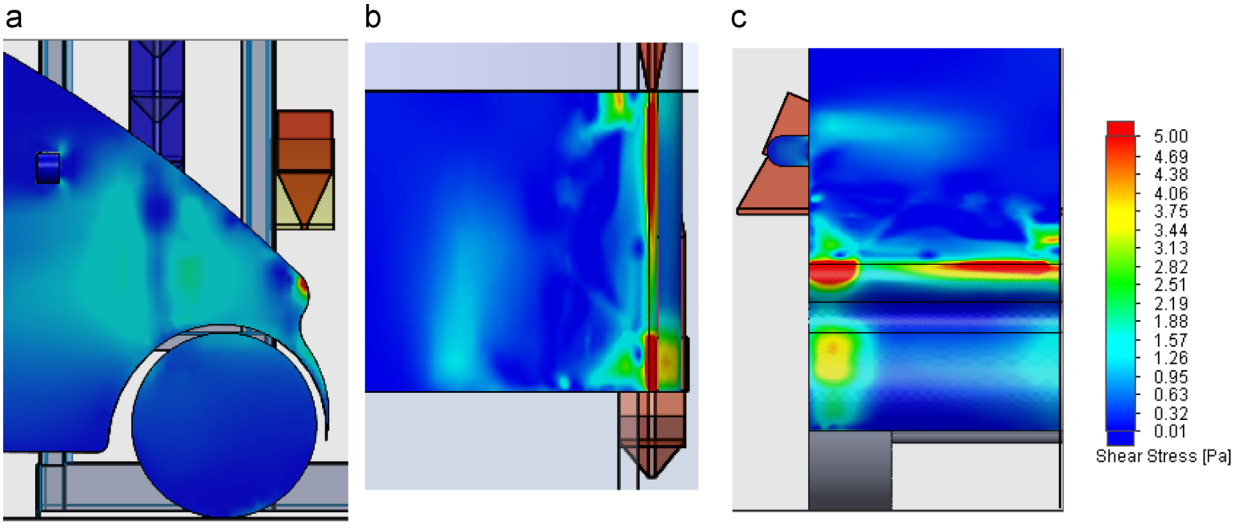

Fig. 23. The shear stress distribution on (a) the lateral and (b, c) frontal surfaces of Smart.

deficiency for the dryers, but a technical constraint, as the horizontal dryer cannot descend any further.

4.3.2. Drying performance on Smart

Fig. 22 illustrates the shear stress distribution on the lateral and roof surfaces of a Mercedes Benz Smart. The shear stress values in these regions range from about 0.9 to 1.5 Pa, which is in the safe area of Fig. 11 for water droplet expulsion.

Similar to Volkswagen pickup van, the immediate impacted regions of the outlets exhibit lower shear stress values as compared to the areas surrounding it. By the passage of the dryer, the regions with lower shear stress will be covered by higher values. It can also be seen from Fig. 22 that shear stress levels on the lateral sides of the Smart vehicle is lower compared to lateral surfaces of Volkswagen, shown in Fig. 21(a). This is mainly due to the shorter width of Smart and hence longer distance from the vertical dryers.

Drying on the roof of Smart is very efficient. The regions near rocker panels and below the doors in this figure exhibit lower shear stress, which is because Smart is closer to the ground level as compared to Volkswagen and therefore they exert lower shear levels.

Fig. 23 presents the shear stress distribution on the lateral and frontal surfaces of Smart vehicle. It can be seen that similar to previous case study; the lateral shear stress level is far above the level provided in Fig. 11 and hence satisfactory for water removal on these surfaces.

It is notable that the drying efficiency depends on the vehicle geometry. Based on the stress distribution results, the new drying system exhibits excellent performance on all horizontal, roof, and upper surfaces of both vehicle representatives. The drying efficiency is satisfactory on most lateral and lower surfaces.

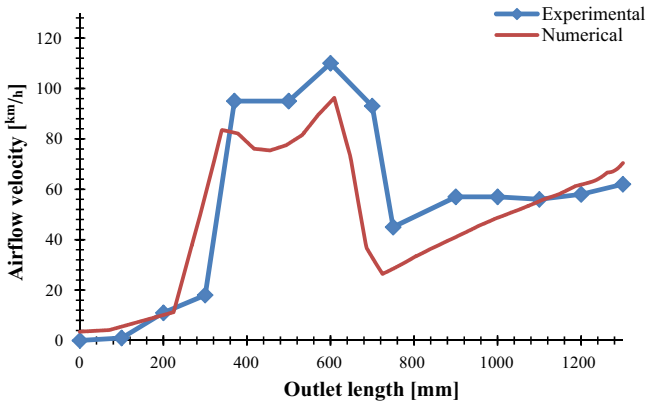

Fig. 24. The numerical and experimental velocity profiles of the horizontal dryer (distance: 150 mm).

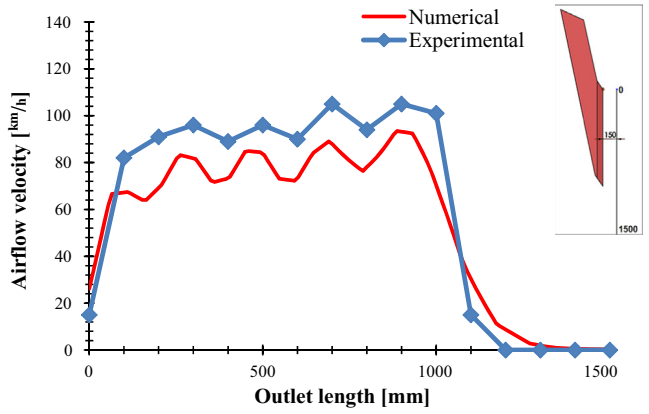

Fig. 25. The numerical and experimental velocity profiles of the vertical dryer (distance: 150 mm).

5. Experimental validation

In order to verify the numerical results, a number of experimental tests were done to measure the airflow velocity along the horizontal and vertical dryers outlets. The numerical and experimental results were then compared to check the accuracy of the results.

In order to measure the airflow velocity of the dryers, a simple digital anemometer was used and moved along the outlets of the dryers (keeping 150 mm distance) and then values were recorded every 100 mm and then plotted.

Fig. 26. The front and rear views of the drying system after installation on the rollover structure.

Fig. 24 shows the airflow velocity profiles obtained from numerical studies and experimental measurements at 150 mm along the outlet of horizontal dryer. As, it can be seen, there is a good agreement between the experimental and numerical results. The average velocity from experimental studies was around 68 km/h, while that of the numerical one was about 57 km/h. The error calculated is about 15%, which could be due to the accuracy of the anemometer used and the difficulties of keeping it at the exact correct position while the dryers are working.

Fig. 25 shows the airflow velocity profiles obtained from numerical studies and experimental measurements at a 150 mm distance along the outlet of vertical dryer. The comparison of experimental and numerical results shows a good agreement. The average velocity from numerical results was about 76.5 km/h, while that from the experimental ones is approximately 87.5 km/h. The error calculated between the two is about 12%.

The accuracy levels of 15% and 12% respectively for horizontal and vertical dryers, is in acceptable range as compared to the results by Martinović et al. [23] where they report an average difference of about 8% and maximum of 15% between the numerical and experimental results for a wood drying process. Also, Levy and Borde [24] report a maximum relative error of 20% among the numerical and experimental results at an outlet of a pipe for a pneumatic drying case study.

There are dryers in the market equipped with retractable, extendable or adjustable blowers such as air discharge units [25] or more specifically car washers with retracting blowers [26]; however, these solutions are available at considerably higher prices and demand sophisticated electro/mechatronic systems. The solution proposed in this work is a simple and inexpensive design proposal that has efficient drying results on various vehicles.

The new drying system was successfully prototyped and its efficiency was checked on various vehicles' geometries. Fig. 26 shows the front and rear views of the first prototype of the drying system after installation on the structure.

The velocity of the machine is dictated by the electric board and powertrain system and is about 10 m/min for the washing passage and approximately 5 m/min in the drying stage (for both with/without flap types). The rollover is first moved in one direction to perform drying, and then in reverse by the actuation of a limit switch disposed at the extremity of the rails. As the result, a passage of drying on a Volkswagen pickup van (with 5 m in length) takes about 60 s, while that on a Smart takes about 30 s.

6. Conclusions

The main objective of this work was to design a new drying system for a rollover carwash machine and additionally to improve the drying efficiency on various vehicle surfaces. After defining the dimensions of the new drying system, numerical studies were done to improve the performance of the dryers, using internal flaps that would direct the airflow to a specific region, to yield a more effective drying for individual dryers. The geometry and optimum position of the internal flaps for the dryers were defined by several studies to yield a better airflow distribution.

The behaviour of the full drying system was studied on actual vehicle models, representative of the shortest and tallest sizes in the car flit market by studying the shear stress distribution on the vehicle surfaces. The results allowed concluding that the overall drying performance of the design system is very good, and assure proper drying on most vehicle surfaces.

Additionally due to size difference between a large and small vehicle, the drying efficiency of a large vehicle is higher than that of a small one, which is mainly due to the distance to the vertical dryers. The drying efficiency on a given vehicle is expected to be in the range of Mercedes Benz Smart and a Volkswagen pickup van, as the smallest and largest vehicles in the market that can be washed with the present carwash machine. The results of this work can be applied to support the design and analysis of other mechanical drying systems.

Acknowledgements

The authors would like to acknowledge the unconditional technical and financial support of *Petrotec* throughout this work. This project was financed by the Portuguese Foundation for Science and Technology, FCT, (SFRH/BD/51105/2010) and FEDER funds through COMPETE 2020 Programme and National Funds under UID/CTM/50025/2013 project.

Annex 1. Fans

The dryer's fans used in this work were centrifugal single-inlet, medium pressure fans. The technical specifications of the fans were as follows:

Model	Velocity (r/min)	Maximum current permissible (A)	Installed power (kW)	Maximum flow (m^3/h)	Sound pressure (dB)	Weight (kg)
CMP-1025-2T-4	2895	10.57	3	2830	77	37.6

Annex 2. Vehicle dimensions

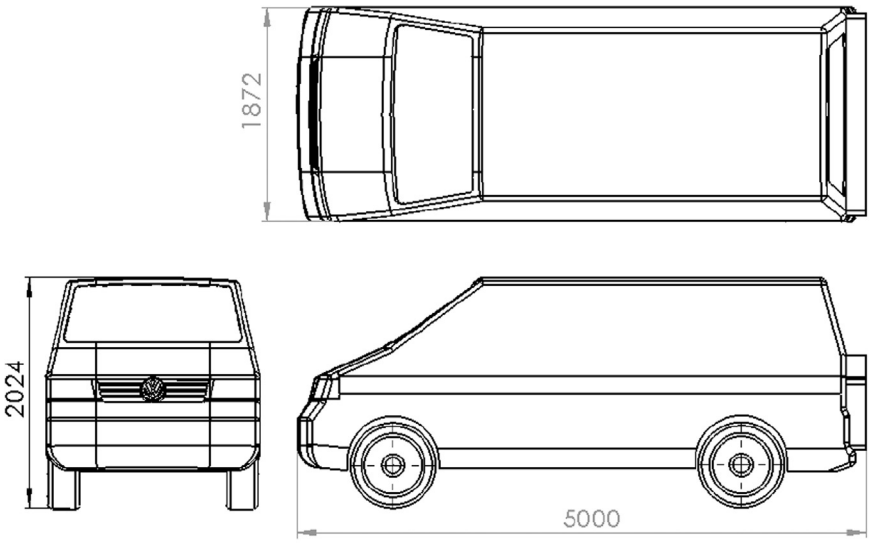

Volkswagen pickup van

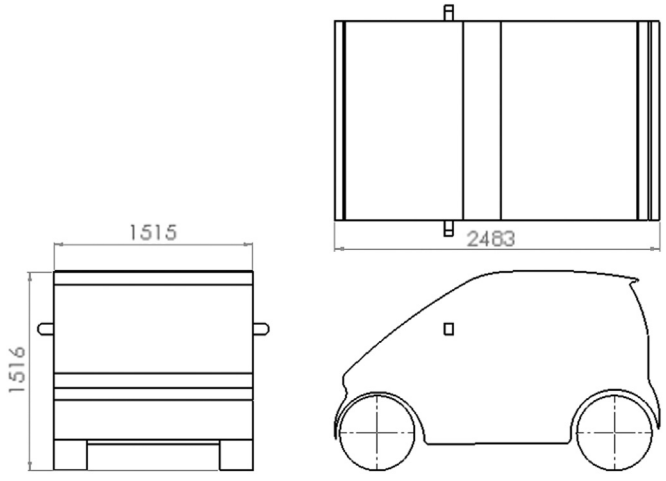

Mercedes Benz Smart

References

[1] Statistic Brain. *Car Wash Industry Statistics* [Internet]. Los Angeles: Statistic Brain Research Institute. Available from: ⟨http://www.statistic-brain.com/car-wash-car-detail-industry-stats/⟩ [updated 02.02.15; cited 26.05.16].

[2] Sabet SMM. *Designing Next Generation Car Washing Machines with Rotary Brushes (Ph.D. thesis)*. Campus de Azurém Guimarães Portugal, University of Minho; 2015.

[3] Cirino JF. *Blower Equipment for Roll-Over Car Wash*. US Patent 3,991,433; 16 November 1976.

[4] Schleeter RH, Schleeter KM. *Drier/Stripper for Car Wash*. US Patent 4,969,272; 13 November 1990.

[5] Larson SL, Prato DJ. *Sherman Industries, Assignee. Dryer for Automatic Car Wash Equipment*. US Patent 4,949,423; 21 August 1990.

[6] Belanger M, Wentworth RJ, Turner BS. *Belanger Incorporation, Assignee. Contour Dryer*. US Patent 5,755,043; 26 May 1998.

[7] Smith CR. *Sherman Industries, Assignee. Control System for Automatic Car Wash Blower*. US Patent 4,995,136; 26 February 1991.

[8] Rodgers L. *Bivens Winchester Corporation, Assignee. Carwash Dryer Control System*. US Patent 4,836,467; 6 June 1989.
[9] Schleeter KM. *Rollover Car Wash with Retracting Cloth Strips*. US Patent 5,339,478; 24 August 1994.
[10] WashTec. *Rollover Car Wash Production* [Internet]. Augsburg Germany: WashTec AG. Available from: ⟨http://www.washtec.no/English.9016.98.html⟩ [cited 26.05.16].
[11] N'guessan HE, White R, Leh A, Baksi A, Tadmor R. Fundamental understanding of drops wettability behavior theoretically and experimentally. In: *Advances in Contact Angle, Wettability and Adhesion*, vol. 1. New York: Wiley Press; 2013. p. 87–96.
[12] Basu S, Nandakumar K, Masliyah J. A model for detachment of a partially wetting drop from a solid surface by shear flow. *J. Colloid Interface Sci.* 1997;**190**(1)253–7.
[13] Theodorakakos A, Ous T, Gavaises M, Nouri JM, Nikolopoulos N, Yanagihara H. Dynamics of water droplets detached from porous surfaces of relevance to PEM fuel cells. *J. Colloid Interface Sci.* 2006;**300**(2)673–87.
[14] Woo MW, Daud WRW, Mujumdar AS, Talib MZM, Hua WZ, Tasirin SM. Comparative study of droplet drying models for CFD modelling. *Chem. Eng. Res. Des.* 2008;**86**(9)1038–48.
[15] Schillberg CH, Kandlikar SG. A review of models for water droplet detachment from the gas diffusion layer-gas flow channel interface in PEMFCs. In: *Proceedings of the Fifth International Conference on Nanochannels, Microchannels and Minichannels,* June 18–20, 2007. Puebla, Mexico; New York: ASME; 2007.
[16] Matsson J. *An Introduction to Solidworks Flow Simulation 2014*. Mission Kansas: SDC Publications; 2014.
[17] CFD Online. *Turbulence Intensity* [Internet]. CFD Online Community. Available from: ⟨http://www.cfd-online.com/Wiki/Turbulence_intensity⟩ [updated 03.01.12; cited 26.05.16].
[18] Day MA. The no-slip condition of fluid dynamics. *Erkenntnis* 1990;**33**(3)285–96.
[19] GoEngineer. *Solidworks Flow Simulation: Solution Adaptive Mesh Refinement* [Internet]. Salt Lake City: GoEngineer. Available from: ⟨http://files.goengineer.com/BestPractices/SolidWorksFlow Simulation Solution Adaptive Mesh Refinement.pdf⟩ [cited 26.05.16].
[20] Shin SC, Yoo IJ, Chun JK. Development of shear stress based sensor to measure drying rate and its application to snack drying automation. In: *Development in Food Engineering*. New York: Springer; 1994. p. 930–2.
[21] Nelson JJ, Alving A, Joseph D. Boundary layer flow of air over water on a flat plate. *J. Fluid Mech.* 1995;**284**:159–69.
[22] Engineering ToolBox. *Air Properties* [Internet]. Available from: ⟨http://www.engineeringtoolbox.com/air-properties-d_156.html⟩ [cited 26.05.16].
[23] Martinović D, Horman I, Demirdžić I. Numerical and experimental analysis of a wood drying process. *Wood Sci Technol* 2001;**35**(1)143–56.
[24] Levy A, Borde I. *Pneumatic and flash drying*. *Handbook of Industrial Drying*, 4th ed., Boca Raton FL: CRC Press; 381–91.
[25] Callahan MD. *Az-Tech Research and Development Corporation, Assignee. Retracting Rotational Backpack Blower Air Discharge Tube Unit*. US Patent 6,125,503; 3 October 2000.
[26] McElroy TP. *Proto-vest Incorporation, Assignee. Car Wash Blower Retract System*. US Patent 6,519,872 B2; 18 February 2003.